Chemical Papers (2022) 76:6551–6556
https://doi.org/10.1007/s11696-022-02347-1

ORIGINAL PAPER

Thermal dissociation kinetics of solid ammonium carbonate for use in NH_3-SCR systems

Sooraj Mohan[1] · **P. Dinesha**[1]

Received: 6 May 2022 / Accepted: 21 June 2022 / Published online: 9 July 2022

Abstract

Selective catalytic reduction (SCR) systems using solid ammonia carriers like carbamates, carbonates, etc., have gained interest in the recent past for NOx abatement from compression ignition engines. Solid ammonia carriers have successfully demonstrated their use in SCR systems. In this experimental study, the thermal dissociation study of ammonium carbonate is made using nonisothermal thermogravimetric analysis. Ammonium carbonate is subjected to three heating rates, Ø of 2, 4, and 8 K/min. The corresponding highest rates of reaction are obtained at temperatures (T_p) of 96, 118, and 128 °C, respectively. At these points, the mass of the samples has been reduced to 1/3rd of the initial mass. From the Arrhenius plots, the average activation energy obtained is 77.39 kJ/mol which is 15% higher than that of ammonium carbamate. An expression for T_p as a function of activation energy, Ø, and order of the reaction is developed using kinetic model. The model can predict the temperatures at which the reaction rates are maximum for a given heating rate.

Keywords Ammonium · NOx · SCR · TGA · Thermal decomposition

List of symbols

ACM	Ammonium carbamate
ACN	Ammonium carbonate
DSC	Differential scanning calorimetry
E_a	Activation energy, J/mol
γ	Rate of reaction, kg/s
m	Mass of sample, kg
m_0	Initial mass of sample, kg
m_F	Final mass of sample, kg
m_T	Mass of sample at temperature T, kg
n	Order of the reaction
Ø	Heating rate, K/min
R	Universal gas constant, 8.314 J/molK
S	Shape index
SCR	Selective catalytic reduction
SSCR	Solid selective catalytic reduction
T	Temperature, K
t	Time, s
TGA	Thermogravimetric analysis
T_p	Temperature at which the rate of reaction is maximum
X	Extent of conversion of solid ammonium salt

Introduction

Selective catalytic reduction (SCR) technology involves the reduction of oxides of nitrogen (NOx) into nitrogen and water by reaction with ammonia (NH_3) on a surface of a catalyst (Mohan et al. 2020). It is widely used in the abatement of NOx from compression ignition engines running on diesel and biodiesel blends (Praveena and Martin 2018). The efficiency in reducing the NOx gases is about 80–90% (Carucci et al. 2009; Jiang et al. 2020; Lao et al. 2020) which makes SCR technology the best viable option for NOx reduction. Currently, urea solution is commonly used in commercial vehicles as an ammonia precursor (Shin et al. 2020). In aqueous urea SCR, the amount of urea converted into ammonia is uncertain. Also, the control of urea injection is complicated and often has problems with deposition inside the pipes at colder temperatures (Börnhorst et al. 2019). Solid ammonium salts are the best alternative to urea solution that act as ammonia carriers that are stable and have higher ammonia release per unit mass. The different ammonia cursors

✉ P. Dinesha
dinesha.p@manipal.edu

[1] Department of Mechanical and Industrial Engineering, Manipal Institute of Technology, Manipal Academy of Higher Education, Manipal 576104, India

for solid-SCR (SSCR) are solid urea, ammine chloride of strontium (Li et al. 2017; Liu and Tan 2020) and calcium, ammonium carbonate, and ammonium carbamate (Kurien and Srivastava 2019). Ammonium carbonate (ACN) and ammonium carbamate (ACM) are the most preferred salts due to their operating temperature range, ease of availability, and storage and can be easily implemented into the current SCR systems (Kim et al. 2014; Peitz et al. 2014). ACN (NH_4–CO_3–NH_4) is a hygroscopic, water-soluble, white crystalline salt, containing a strong odor of ammonia. Upon heating, the salt converts initially into ammonium bicarbonate which further decomposes to carbon dioxide and water. The molecular weight of ACN and ACM are 96.09 and 78.07 g/mol, respectively (Peitz et al. 2014). The ammonia storage capacity is, respectively, 20.8 mol and 25.8 mol per kg (Fulks et al. 2009; Kim et al. 2014). In terms of mass, NH_3 gas of 0.35 g and 0.436 g is obtained from 1 g of ACN and ACM, respectively. ACM is preferred to ACN for NH_3-SCR as it does not generate H_2O and a better pressure of NH_3 is developed easily at lower temperatures. NH_3/CO_2 ratio is an important factor to be considered as both these gases can combine and readily form a carbamate (Fulks et al. 2009). Kim et al. have investigated the thermal degradation study of ACM and assessed its effect on the pressure release (Kim et al. 2020). However, in their study, only a single heating rate of 5 K/min was used and the effect of different rates of heating was not analyzed. Very few studies have addressed the investigation of solid ammonium carbonate as an ammonia carrier for SCR systems. Also, lacuna exists in terms of the experimental data regarding thermal dissociation parameters of ACN. Changes in the heating rate have significant effects on the reaction rates and temperature at which the rate is a maximum. This paper aims to estimate the activation energy of ammonium carbonate using TGA/DSC analysis and compare the results obtained with ammonium carbamate. The comparison shall provide insights as to which compound is more suitable for use in NH_3-SCR systems. Also, relationship between the heating rate and the temperature at which the highest rate of reaction is observed will be derived.

Kinetics of dissociation

Thermal dissociation of ammonium carbonate

The dissociation of ammonium carbonate can be kinetically modeled using the reaction rate of the salt using Arrhenius constants (Mohan and Dinesha 2022). The solid salt sublimates to ammonia gas due to the application of heat and the rate of the reaction can be represented as a product of two parameters given by Eq. (1) (Fogler 2006).

$$\gamma = -\frac{\mathrm{d}m}{\mathrm{d}t} = Am_0(1-X)^n e^{-E_a/\mathrm{RT}} \tag{1}$$

where γ is the rate of the reaction, A is the pre-exponential (frequency) factor in s^{-1}, E_a is the activation energy in J/mol, and R is the universal gas constant, 8.314 J/mol−K. X is the fraction of the salt converted to gas. The order of the reaction, n, is obtained using the shape index as discussed by Kissinger (1957). The slope $-\frac{\mathrm{d}m}{\mathrm{d}t}$ is calculated using finite difference approximation of the order $O\left(\Delta t^2\right)$ (central differencing).

Experimental setup

ACN is a colorless, crystalline solid having a molecular formula, $(NH_4)_2CO_3$, and a molecular weight of 96 g/mol which is soluble in water. The ACN samples of laboratory reagent grade were locally procured which had a purity of more than 98%. Its density is 1,500 kg/m^3 and had a melting point of 58 °C. Thermogravimetric analysis (TGA) was carried out in this study using a Q50 analyzer. The samples were taken into the test chamber, which was filled with nitrogen gas. Three separate samples (Sample 1, 2, and 3) were subjected to different heating rates, Ø of 2 K/min, 4 K/min, and 8 K/min, respectively, to ascertain the weight loss of ACN. The amount of mass lost due to thermal degradation was measured against time. The resulting data were used to estimate the average activation energy and pre-exponential factor for dissociation of ACN. Another separate sample (Sample 4) was taken into a Q200 analyzer for differential scanning calorimetry. The sample was heated in the test chamber filled with nitrogen gas. Changes in the heat flow were measured against the temperature rise. The result of DSC was used to assess the stability of ACN and to identify the shape index for determining the order of the reaction. Weights of samples 1, 2, 3, and 4 measured 11.324 mg, 14.677 mg, 15.976 mg, and 4.2 mg, respectively.

Results and discussion

DSC analysis

Sample 4 was taken into DSC Q200 and checked for endothermic behavior. Figure 1 shows the heat flow against temperature for a heating rate of 4 K/min. The DSC curve is now used to identify the shape index of the peak formation, using the values of a and b as shown in Fig. 1. From Fig. 1, the shape index, S is calculated as $\frac{a}{b} = 0.29$ (Kissinger 1957;

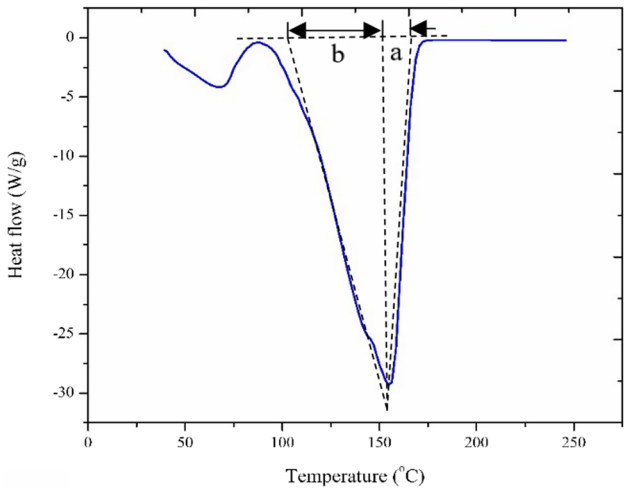

Fig. 1 A graph of endothermic heat flow against temperature for ammonium carbonate obtained from differential scanning calorimetry (DSC)

Simon Fraser University 2013), and further the order of the reaction, n is calculated as $n = 1.26\sqrt{S} = 0.6825$. This value is further used in kinetics equations for estimating the activation energy.

TGA analysis

Samples 1, 2, and 3 were subjected to TGA for heating rates of 2, 4, and 8 K/min, respectively. Figure 2a shows the conversion of the salts from room temperature. The final mass of the salts corresponding to 2, 4, and 8 K/min was 0.00015 mg, 0.00026 mg, and 0.00018 mg, respectively. Figure 2b shows the derivative weight (in %/K) indicating the maximum peak temperatures (T_p) at which the slope changes its sign. The derivative plot indicates the point of the greatest rate of change against temperature on the weight loss curve. From the figure T_p values for samples 1, 2, and 3 are 95.98 °C, 118.3 °C, and 128.15 °C, respectively. At these temperatures, the rate of change of mass of the salts is a maximum. This data are useful in controlling the rate of reaction ACN using heating rate and operating temperature. For example, when a high release of ammonia is desired, with an available heating rate of 4 K/min, ACN will have to be operated in the vicinity of 118 °C, which is the T_p at that heating rate. Figure 3 shows the Arrhenius plot of $\ln\left[\left(-\frac{dm}{dt}\right)\left(\frac{1}{m_0(1-X)^n}\right)\right]$ against $1000/T$. A first-order linear equation is fitted to each heating rate. The fitted line had high values of R^2 of 0.9922, 0.9967, and 0.9971. The slope and intercept of the fitted regression model are used to calculate the activation energy and pre-exponential factor that are shown in Table 1. Even when the material and the reaction are the same, the literature has shown that there is a difference in activation energy with respect to heating rate (Dingcheng et al. 2018).

The results obtained are similar to the values obtained by Lee et al. (2013) who obtained activation energy of 75.49 kJ/mol. Fulks et al. (2009) have reported that the ammonia release energy from ammonium carbonate is 109 kJ/mol. The rate of the reaction for ACN can be thus be derived as

$$\gamma = -\frac{dm}{dt} = m_0\left(8.88X10^7\right)(1-X)^{0.6825}e^{-9308.4/T} \quad (15)$$

In the current study, the highest rate of reaction obtained for the heating rates of 2, 4, and 8 K/min is obtained at temperatures of 95, 117, and 126 °C, respectively. The corresponding salt conversion (X) is obtained as 0.64, 0.68, and 0.67, respectively. Figure 2b shows the derivative plot that shows the peak temperature T_p. The peak temperature

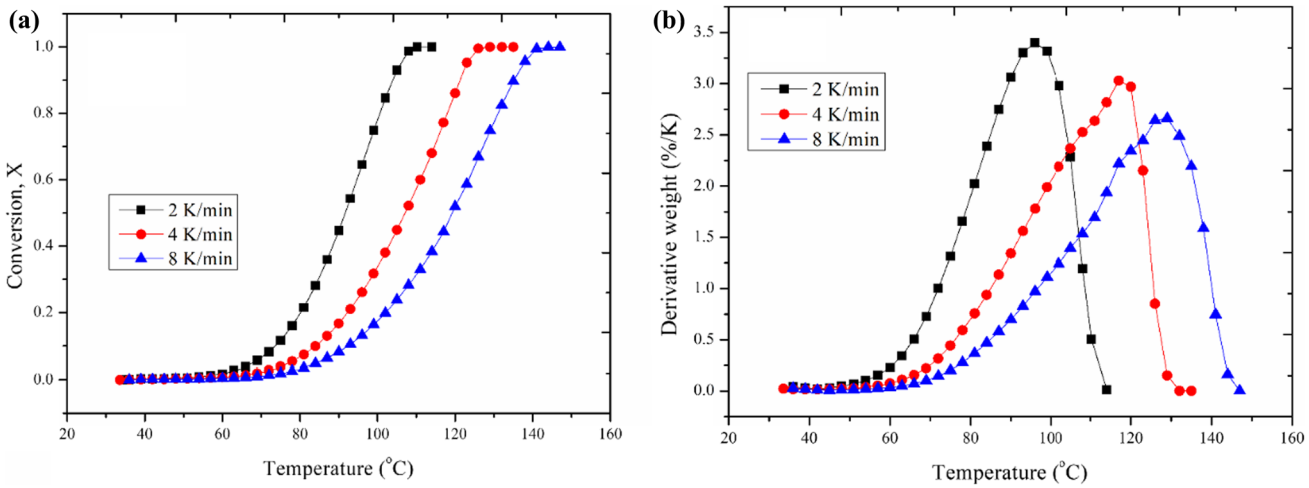

Fig. 2 **a** Extent of conversion, X and **b** derivative plot obtained from thermogravimetric analysis of ammonium carbonate

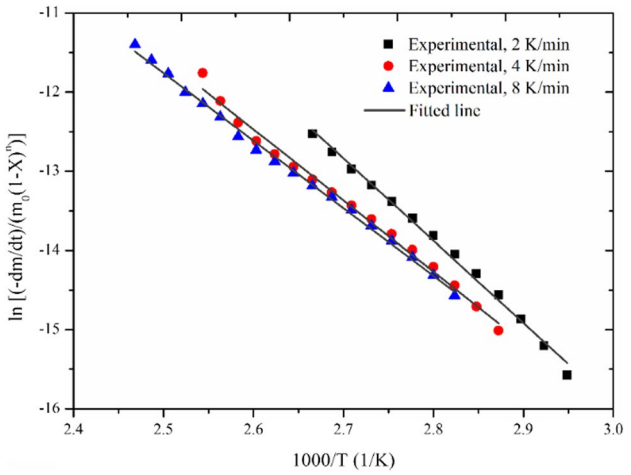

Fig. 3 Arrhenius plot obtained for three different heating rates and the fitted linear equation

Table 1 Activation energy and pre-exponential factor obtained for ammonium carbonate

Heating rate, Ø (K/min)	Activation energy (kJ/mol)	Pre-exponential factor (s^{-1})	R^2 value for the fitted equation
2	86.44	1.51×10^8	0.9922
4	74.75	7.05×10^7	0.9967
8	70.99	4.49×10^7	0.9971
Average	77.39	8.88×10^7	

corresponds to a point where the derivative of $\left(-\frac{dm}{dt}\right)$ changes its sign. The values of T_p obtained for 2, 4, and 8 K/min are 96, 118, and 128 °C, respectively. These temperatures are the same as that seen for the highest rate of reaction. Also, the values of T_p and the highest rate of dissociation are observed when the extent of conversion, is about 66% ($X_p = 0.66$) of the initial mass. It can be concluded that the peak temperature is obtained when the mass of the sample is reduced to 1/3rd of the initial mass ($m_p = m_0/3$); or $(1 - X_p) = 1/3$.

The peak temperature is observed when the slope $-\frac{dm}{dt}$, reverses the sign. It can be obtained by differentiating Eq. (1) with respect to time and equating it to zero as shown in Eq. (2).

$$\frac{d}{dt}\left(-\frac{dm}{dt}\right) = \frac{d}{dt}\left[Am_0 e^{-\frac{E_a}{RT}}(1-X)^n\right] \tag{2}$$

On further simplification, Eq. (2) reduces to

$$0 = Am_0 e^{-\frac{E_a}{RT_p}}(1-X_p)^n\left[\frac{n}{(1-X_p)}\left(-\frac{dX}{dt}\right)_p + \frac{E_a \emptyset}{RT_p^2}\right] \tag{3}$$

$$\frac{n}{(1-X_p)}\left(\frac{dX}{dt}\right)_p + \frac{E_a \emptyset}{RT_p^2} = 0 \tag{4}$$

$\left(\frac{dX}{dt}\right)_p$ is the rate of the extent of conversion at the peak temperature T_p. By substituting the value, $(1 - X_p) = 1/3$, and rearranging, we can get an expression for T_p as a function of $\left(\frac{dX}{dt}\right)_p$ as

$$T_p = \sqrt{\frac{E_a \emptyset}{3Rn\left(\frac{dX}{dt}\right)_p}} \tag{5}$$

The peak temperatures obtained for heating rates 2, 4, and 8 K/min are 96, 118, and 128 °C, respectively. The derivative of conversion with respect to time, $\frac{dX}{dt}$, at these peak temperatures is calculated using central differencing equations as 0.0011, 0.002, 0.0036 s^{-1}, respectively. The slopes of $\left(\frac{dX}{dt}\right)_p$ showed a linear relationship with the heating rates. To simplify the expression further, $\left(\frac{dX}{dt}\right)_p$ is expressed as a function of Ø as shown in Eq. (6).

$$\left(\frac{dX}{dt}\right)_p = 0.0251\emptyset + 0.0003 \tag{6}$$

Equation (6) is a simple linear approximation of $\left(\frac{dX}{dt}\right)_p$ as a function of Ø and hence is associated with errors. A correction factor is now introduced $(12.48 - 96.87\emptyset)$, which is also a function of Ø and appended to Eq. (20). Hence the equation for T_p for $\emptyset = (2, 8)$ is now modified as

$$T_p = (12.48 - 96.87\emptyset) + \sqrt{\frac{E_a \emptyset}{3Rn(0.0251\emptyset + 0.0003)}} \tag{7}$$

The values of T_p estimated using Eq. (7) for heating rates of 2, 4, and 8 K/min are 95.54, 118.67, and 127.77 °C, which is very close to the experimentally obtained peak temperatures. With the known values of activation energy and shape index, the peak temperature for a given heating rate can be estimated or vice versa. This approach is very helpful in designing the heating circuit in the SCR system.

The activation energy obtained in this work is compared with the results of Kim's study (Kim et al. 2020) on ACM. Figure 4 shows the comparison of conversion obtained in the current work with results obtained from Kim et al. (2020). ACM decomposes completely for a heating rate of 5 K/min. In comparison, a similar curve is obtained for ACN decomposition in the current study for a slower heating rate of 2 K/min. Prima facie shows that degradation of ACN occurs at a lower ramp rate of heating as compared to ACM. Considering the waste heat available from hydrocarbon combustion, this information is useful for implementing Solid

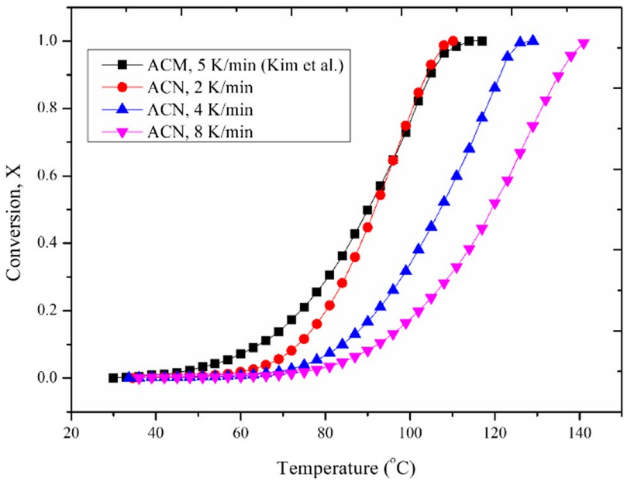

Fig. 4 TGA curves of ACN from the present study in comparison with ACM (Kim et al. 2020)

SCR systems. NH_3 release energy for ACN is also higher compared to that of ACM (Fulks et al. 2009). For ACN, the solid to gas reaction involves one additional mole of water vapor also as a product. Hence, the activation energy would be higher than that of ACM. The values of activation energy for ACM reported in the literature are between 57.2 and 66.9 kJ/mol (Y. Kim et al. 2020; Lee et al. 2013) which are lower than ACN. Hence, ACN requires a much rapid heating rate as compared to ACM for the same rate of conversion.

ACM also has a higher partial pressure of NH_3 compared to ACN. ACM can produce 15% (vol.) more NH_3 vapors than ACN for the same heat available. Another important factor is that the solid reaction of ACN produces one mole of water vapor which is absent in the case of ACM dissociation. The combustion products will be carrying water vapors in the exhaust line and it will form deposits on the inner surfaces. This condition is persistent even if ACM is used as the precursor. In terms of cost, ACM is expensive by at least 2.5–3 times the cost of ACN, which is significant.

Conclusions

This paper experimentally investigates the thermal degradation and chemical kinetics studies of ammonium carbonate as a solid ammonia carrier for use in an NH_3-SCR system in a CI engine. The rate of the reaction is obtained as

$$\gamma = -\frac{\mathrm{d}m}{\mathrm{d}t} = m_0\left(8.88 \times 10^7\right)(1-X)^{0.6825} e^{-9308.4/T}$$

The highest rate of the reactions is obtained when the mass of the sample is reduced to 1/3rd of the initial mass at a temperature T_p. Expression for peak temperature, T_p for heating rates, $\emptyset = (2, 8)$ is derived and calculated. This enables the estimation of the peak temperature regime for any given heating rate.

Acknowledgements The authors thank the Vision Group on Science and Technology (VGST), Government of Karnataka, India, for funding the project (vide grant no. GRD-911). The open-access funding for this article is provided by Manipal Academy of Higher Education, Manipal.

Author contributions SM contributed to conceptualization, methodology, investigation, formal analysis, and writing—original draft. PD contributed to validation, visualization, supervision, and writing—review and editing.

Funding Open access funding provided by Manipal Academy of Higher Education, Manipal.

Data availability Data will be made available on request.

Declarations

Conflict of interest There are no competing or conflicts of interest to declare.

References

Börnhorst M, Langheck S, Weickenmeier H, Dem C, Suntz R, Deutschmann O (2019) Characterization of solid deposits from urea water solution injected into a hot gas test rig. Chem Eng J 377:119855. https://doi.org/10.1016/j.cej.2018.09.016

Carucci JRH, Kurman A, Karhu H, Arve K, Eränen K, Wärnå J, Salmi T, Murzin DY (2009) Kinetics of the biofuels-assisted SCR of NOx over Ag/alumina-coated microchannels. Chem Eng J 154(1):34–44. https://doi.org/10.1016/j.cej.2009.01.031

Dingcheng L, Qiang X, Guangsheng L, Junya C, Jun Z (2018) Influence of heating rate on reactivity and surface chemistry of chars derived from pyrolysis of two Chinese low rank coals. Int J Min Sci Technol 28(4):613–619. https://doi.org/10.1016/j.ijmst.2018.05.001

Fogler HS (2006) Elements of chemical reaction engineering. Prentice Hall PTR. https://books.google.co.in/books?id=QLt0QgAACAAJ

Fulks G, Fisher GB, Rahmoeller K, Wu M-C, D'Herde E, Tan J (2009) A review of solid materials as alternative ammonia sources for lean NOx reduction with SCR. SAE Technical Paper2, 2009-01–09

Jiang L, Cai Y, Jin M, Zhu Z, Wang Y (2020) The Influence of Ce or Mn doping on Cu-based catalysts for De-NOx with NH3-SCR. J Chem 2020:1462801. https://doi.org/10.1155/2020/1462801

Kim Y, Raza H, Lee S, Kim H (2020) Study on the thermal decomposition rate of ammonium carbamate for a diesel NOx reducing agent-generating system. Fuel 267:117306. https://doi.org/10.1016/j.fuel.2020.117306

Kim H, Yoon C, Lee J, Lee H (2014) A study on the solid ammonium SCR system for control of diesel nox emissions. SAE Technical Paper, 2014-01–15

Kissinger HE (1957) Reaction kinetics in differential thermal analysis. Anal Chem 29(11):1702–1706. https://doi.org/10.1021/ac60131a045

Kurien C, Srivastava AK (2019) Solid reductant based selective catalytic reduction system for exhaust emission control of compression ignition engines. Nat Environ Pollut Technol 18(3):969–973

Lao CT, Akroyd J, Eaves N, Smith A, Morgan N, Nurkowski D, Bhave A, Kraft M (2020) Investigation of the impact of the configuration of exhaust after-treatment system for diesel engines. Appl Energy 267:114844. https://doi.org/10.1016/j.apenergy.2020.114844

Lee H, Yoon C, Kim H (2013) A study on reaction rate of solid scr for nox reduction of exhaust emissions in diesel engine. Trans Korean Soc Autom Eng 21(6):183–194. https://doi.org/10.7467/ksae.2013.21.6.183

Li J, Ge Y, He C, Tan J, Peng Z, Li Z, Chen W, Wang S (2017) The application of solid selective catalytic reduction on heavy-duty diesel engine. SAE Technical Paper. https://doi.org/10.4271/2017-01-2364

Liu Y, Tan J (2020) Experimental study on solid SCR technology to reduce NOx Emissions From Diesel Engines. IEEE Access 8:151106–151115. https://doi.org/10.1109/ACCESS.2020.3016959

Mohan S, Dinesha P (2022) Global kinetic modeling of low-temperature NH3-SCR for NOx removal using Cu-BEA catalyst. Mater Today Proc 52:1321–1325. https://doi.org/10.1016/j.matpr.2021.11.062

Mohan S, Dinesha P, Kumar S (2020) NOx reduction behaviour in copper zeolite catalysts for ammonia SCR systems: a review. Chem Eng J 384:123253. https://doi.org/10.1016/j.cej.2019.123253

Peitz D, Bernhard A, Krocher O (2014) Ammonia storage and release in SCR systems for mobile applications. In: Nova I, Tronconi E (eds) Urea-SCR technology for deNOx after treatment of diesel exhausts. Springer, pp 485–506

Praveena V, Martin MLJ (2018) A review on various after treatment techniques to reduce NOx emissions in a CI engine. J Energy Inst 91(5):704–720. https://doi.org/10.1016/j.joei.2017.05.010

Shin Y, Jung Y, Cho CP, Pyo YD, Jang J, Kim G, Kim TM (2020) NOx abatement and N2O formation over urea-SCR systems with zeolite supported Fe and Cu catalysts in a nonroad diesel engine. Chem Eng J 381:122751. https://doi.org/10.1016/j.cej.2019.122751

Simon Fraser University (2013) Kinetics of decomposition of sodium bicarbonate; a Differential Scanning Calorimetry experiment. In Simon Fraser University. http://www.sfu.ca/~brodovit/files/chem366/manual/09_dsc131.pdf